Mechanism of metal ion activation of the diphtheria toxin repressor DtxR

J. Alejandro D'Aquino[†], Jaclyn Tetenbaum-Novatt[†], Andre White[‡], Fred Berkovitch[†], and Dagmar Ringe[†§]

[†]Departments of Chemistry and Biochemistry and Rosenstiel Basic Medical Sciences Research Center, Brandeis University, Waltham, MA 02454; and [‡]Department of Medicinal Chemistry, Boehringer Ingelheim Pharmaceuticals, Ridgefield, CT 06877

Edited by Gregory A. Petsko, Brandeis University, Waltham, MA, and approved October 3, 2005 (received for review February 25, 2005)

The diphtheria toxin repressor (DtxR) is a metal ion-activated transcriptional regulator that has been linked to the virulence of *Corynebacterium diphtheriae*. Structure determination has shown that there are two metal ion binding sites per repressor monomer, and site-directed mutagenesis has demonstrated that binding site 2 (primary) is essential for recognition of the target DNA repressor, leaving the role of binding site 1 (ancillary) unclear. Calorimetric techniques have demonstrated that although binding site 1 (ancillary) has high affinity for metal ion with a binding constant of 2×10^{-7}, binding site 2 (primary) is a low-affinity binding site with a binding constant of 6.3×10^{-4}. These two binding sites act in an independent fashion, and their contribution can be easily dissected by traditional mutational analysis. Our results clearly demonstrate that binding site 1 (ancillary) is the first one to be occupied during metal ion activation, playing a critical role in stabilization of the repressor. In addition, structural data obtained for the mutants Ni-DtxR(H79A,C102D), reported here, and the previously reported DtxR(H79A) have allowed us to propose a mechanism of metal activation for DtxR.

iron | homeostasis | transcription regulation

The diphtheria toxin repressor (DtxR) is a member of a family of metal ion-regulated repressors that control transcription of virulence genes in pathogenic bacteria. Crystallographic studies of DtxR have shown that the active form of the repressor is a homodimer consisting of two domains (1). The N-terminal domain contains the helix–turn–helix motif responsible for DNA binding and two binding sites for metal ion (2). The function of the C-terminal domain is not completely understood, but it is not likely to play an essential role in activation of the repressor because gel mobility shift assays show that a DtxR mutant lacking the C-terminal domain binds DNA with the same affinity as wild type (WT) (3). In addition, there are members of the DtxR family that naturally lack this domain (4). Mutagenesis experiments have shown that alanine (Ala) substitution of any of the ligands of binding site 2 (primary) results in an inactive mutant that no longer binds to its operator DNA (5, 6). The interpretation of similar experiments on binding site 1 (ancillary) has not been as clear. Early mutational studies show small decreases in activity and suggest that this site is expendable (5). More recent *in vivo* studies determined that a minimum of two Ala substitutions in this site are required to abolish activity of the repressor (6). Lately, the effects of Ala substitution of ligands corresponding to binding site 2 (primary) in WT and the DtxR(E175K) mutant has been revisited by using a novel *in vivo* assay. These studies suggest that binding site 1 (ancillary) is critically involved in activation of DtxR (7).

In addition to ferrous ion, DtxR is activated by other divalent transition metal ions *in vitro* with the following order of activation: $Fe^{2+} \sim Ni^{2+} > Co^{2+} \gg Mn^{2+}$ (8, 9). Early binding experiments showed that DtxR has a high-affinity metal ion binding site with an affinity for Ni^{2+} between 2.11×10^{-6} and 9×10^{-7} (10, 11). The shape of the binding curves led the researchers to infer that metal ion binding to DtxR is cooperative (11). Reconstitution experiments were unable to determine relative binding affinities but established that binding site 1 (ancillary) has a higher affinity for metal ion than binding site 2 (primary) (8). These results led the authors to suggest that there is some cooperativity in metal ion binding between the sites and/or that there is increased stability of the protein by having two occupied metal-binding sites (8).

NMR studies have shown that metal ion binding results in ordering of the N-terminal domain with minimal changes in secondary structure (12). Recently, a set of relative binding affinities was measured calorimetrically, and an activation mechanism was proposed (3). This mechanism suggests that alignment of the DNA binding helices after metal ion binding to binding site 2 (primary) is the key event during activation (3). Following that step, coordination to binding site 1 (ancillary) results in formation of the binding interface and completes ordering of the N-terminal domain (3). This mechanism contrasts with some of the experimental evidence found in the literature. Rangachari *et al.* (3) found that binding site 1 (ancillary) deficient mutants coordinate a single equivalent of metal ion and this coordination occurs in binding site 2 (primary). Following the logic presented in the proposed mechanism by Rangachari *et al.* (3), a binding site 1 (ancillary) mutant such as DtxR(H79A) would be unable to go through the dimerization step, which would make it inactive (3). However, this mutant, like the rest of the single Ala mutants of binding site 1 (ancillary), is active both *in vivo* and *in vitro* (3, 5, 6).

To address these issues, we have designed a self-consistent system including WT DtxR and the mutants DtxR(H79A) (metal ion binding site 1), DtxR(C102D) (metal ion binding site 2), and DtxR(H79A,C102D) (both sites mutated) to study the activation of DtxR by metal ion using crystallographic and calorimetric techniques. We have measured the metal ion-binding affinities of these proteins calorimetrically and determined the effect that each mutation has on both metal ion-binding sites as well as potential cooperative effects between them. We also have determined the crystal structure of Ni-DtxR(H79A,C102D) [Protein Data Bank (PDB) ID code 1XCV] and used it in conjunction with the previously reported structures of WT DtxR (1BIO) and the mutants DtxR(H79A) (1P92) and Ni-DtxR(C102D) (2TDX) to correlate conformational changes with differences in metal ion coordination at both binding sites. We have used differential scanning calorimetry (DSC) to study the thermal stability and oligomerization state of DtxR in the presence and absence of metal ion. Our results have allowed us to isolate important events during metal ion activation of DtxR and to propose a molecular mechanism that fits all of the available data. Finally, we have investigated the nature of the reported chemical modification to Cys-102 during crystallization using mass spectrometry in combination with crystallographic techniques (2, 5).

Conflict of interest statement: No conflicts declared.

This paper was submitted directly (Track II) to the PNAS office.

Abbreviations: DSC, differential scanning calorimetry; DtxR, diphtheria toxin repressor; PDB, Protein Data Bank.

Data deposition: The atomic coordinates and structure factors have been deposited in the Protein Data Bank, www.pdb.org (PDB ID code 1XCV).

§To whom correspondence should be addressed. E-mail: ringe@brandeis.edu.

Table 1. Data collection and refinement statistics

Data collection	
Observed reflections	67,517
Unique reflections	13,359
Signal to noise $I/\sigma_{(I)}$ overall/hrs	10.7/2.9
Redundancy, overall/hrs	5.1/3.5
R_{merge}, overall/hrs	0.05/0.2
Temperature, K	100
Completeness, %	90.4
Refinement	
Unit cell	
$a = b, c$, Å	63.1, 106
$\alpha = \beta, \gamma$, °	90, 120
Space group	$P3_121$
Resolution, Å	26 – 2.1
R factor/R_{free}	26/33
R factor$_{(hrs)}$	30
Nonhydrogen atoms	1,170
rms bonds, Å	0.006
rms angles, °	1.1

hrs, high-resolution shell.

Materials and Methods

Protein Purification and Crystallization. Initial protein samples of WT DtxR and the mutants DtxR(H79A) (binding site 1), DtxR(C102D) (binding site 2), and DtxR(H79A,C102D) were obtained from John Murphy (Boston University School of Medicine, Boston). Recently, protein samples have been overexpressed and purified in our laboratory as described in ref. 7. All protein samples were dissolved in 0.1 M Tris (pH 7.5) (work buffer). Samples of WT DtxR and mutants containing Cys-102 were kept in solutions with added 20 mM DTT or 2-mercaptoethanol in the work buffer. Protein samples used for crystallization were incubated with 5 mM $NiCl_2$ and concentrated to 10–16 mg/ml, and later crystallized by vapor diffusion using the hanging drop method at room temperature. The protein solution (5 μl) was mixed with an equal amount of well solution [2.8 M $(NH_4)_2SO_4$, 0.1 M Tris (pH 7.5), 5 mM $NiCl_2$, and 6% poly(ethylene glycol) 400]. Crystals suitable for crystallographic analysis were harvested from the drops after 2 weeks. The crystals were $\approx 0.2 \times 0.2 \times 0.4$ mm^3 in size.

Data Collection. The data for Ni-DtxR(H79A,C102D) were collected at the National Synchrotron Light Source at Brookhaven National Laboratory on the X12C beamline equipped with a charge-coupled device detector (Brandeis University, Waltham, MA). The data were collected to a maximal resolution of 2.1 Å. The crystals belong to space group $P3_121$ with unit cell dimensions of a = b = 63.1 Å, c = 106.0 Å, $\alpha = \beta = 90°$, $\gamma = 120°$. The data were scaled and integrated by using the programs DENZO and SCALEPACK of the HKL suite and D*TREK (13, 14). Statistics for the data collection are presented in Table 1.

Structure Determination and Refinement. The structure of Ni-DtxR(H79A,C102D) was solved by molecular replacement with the program EPMR (15) using the coordinates of Ni-Dtxr(C102D) (PDB ID code 2TDX) as search model (5). A round of rigid body refinement was followed by several rounds of manual building and positional refinement using the programs O and CNS (16–18). The quality of the model was monitored by using PROCHECK (19, 20). After each round of refinement, new difference Fourier electron density maps were generated. Simulated annealing omit maps were generated to help the interpretation of the electron density and reduce bias introduced by initial placement of the model (21). The structure of Ni-DtxR(H79A,C102D) showed four nonglycine residues outside traditionally allowed regions of the Ramachandran plot, consistent with previous structures of WT DtxR (1, 22–24). The existence of such conformations has been validated in cases where they lead to stabilization of the structure (25). Complete statistics for the refinement are shown in Table 1. The relatively high R-factor exhibited by the model of Ni-DtxR(H79A,C102D) reflects the unaccounted-for scattering of the C-terminal domain, which, although not visible in the electron density map, is part of the sequence.

Mass Spectrometry. Mass spectrometry data for DtxR(H79A) were acquired at the Boston University School of Medicine Mass Spectrometry Resource on a Quattro II triple quadrupole mass spectrometer (Micromass, Manchester, U.K.) operating in the MS1 (first quadrupole only) mode. Ions were generated by using 1.0-μm nanoelectrospray tips purchased from New Objective (Woburn, MA), and 1.02-kV voltage was applied via an internal electrode. Samples were ≈ 5 μM in 85:15 0.1% aqueous methanol:formic acid (vol/vol). The resulting mass spectra were analyzed by using MAXENT software supplied with the instrument (MASSLYNX, Version 3.4, Waters) to calculate the reconstructed neutral mass of the proteins being analyzed.

Isothermal Titration Calorimetry. Isothermal titration calorimetry experiments were performed on a VP-ITC calorimeter (Microcal, Northampton, MA) at a 25°C. Freshly prepared protein samples were dialyzed to avoid any interference from the DTT present and degassed before the experiments. Protein samples of concentration 50–70 μM were titrated against 0.1 M Tris buffer (pH 7.5) containing concentrations of $NiCl_2$ in the range of 0.1–20 mM. Because 0.1 M Tris (pH 7.5) is the most commonly used buffer used in *in vitro* work on DtxR, this buffer was used for all experiments. However, experiments done only in one buffer yield relative rather than absolute binding affinities. Complete saturation of the low-affinity binding site required larger titrant concentrations. The data were fitted by using Microcal ORIGIN software supplied with the instrument. Titrations of samples containing Cys-102 yielded the largest errors, presumably because of partial derivatization of Cys-102 during manipulation of the samples.

DSC. DSC experiments were performed on a VP-DSC calorimeter (Microcal) using a scan rate of 1°C/min. DSC traces were recorded for protein samples with concentrations ranging from 1 to 5 mg/ml, previously incubated or not with metal ion. In all cases, the samples were dialyzed against the appropriate buffer and degassed prior to the experiment. The choice of buffer depended on the pH of the experiment and the salt concentration. For experiments at pH 7.5, the work buffer was used; for pH 4.5, 0.1 M sodium formate buffer was used. High-salt experiments were performed using conditions identical to those used for crystallization. Thermally induced folding–unfolding transitions correspond to raw data. Differences in transition temperature of the observed thermally induced folding–unfolding profiles were used directly as a measure of protein stability. To determine the oligomerization state of DtxR, DSC experiments were repeated using protein concentrations ranging from 0.5 μM to 0.5 mM. The lower limit of concentration approaches the detection limit of the instrument. In this range of concentrations, the transition temperatures observed for thermal denaturation curves of apo-DtxR at different protein concentrations were identical.

Results and Discussion

Structure of Ni-DtxR(H79A,C102D). The structure of the double metal ion-binding-site mutant Ni-DtxR(H79A,C102D) does not show any structural perturbations caused by the mutations in or around the binding sites. We compared the structural similarities and differences found in the binding sites of Ni-DtxR(H79A,C102D) and the previously reported DtxR(H79A) with other DtxR structures (23). The structure of Ni-DtxR(H79A,C102D) shows clear electron density for residues 1–139 with a calculated overall B-factor of 32

Table 2. Metal ion–ligand distances in binding site 2 (primary)

Ligand	Ni-DtxR H79A C102D activated, Å	Ni-DtxR C102D DNA (1DDN) complex, Å	Ni-DtxRC102D (2DTX) activated, Å
Met-10 S	2.5	2.2	2.7
Asp-102 O	2.0	2.0	2.2
Asp-102 Oδ	2.0	2.1	2.3
Glu-105 Oε	2.1	2.3	2.2
His-106 Nε	2.2	2.2	2.5
Water	2.0	2.0	2.4

Å^2. The quality of the electron density did not allow building of the C-terminal domain.

Structural alignments of the N-terminal domain of Ni-DtxR(H79A,C102D) with those of structures of metal-free WT and metal-bound WT and mutants, both with and without DNA {metal-free WT DtxR [PDB ID code 1DPR (26)], metal-free and zinc-bound WT DtxR [1BI0 and 1BI1 (27)], nickel-bound DtxR(C102D) [2TDX (5)], cobalt-bound WT DtxR [2DTR (28)], cobalt- and DNA-bound WT DtxR [1COW (29)], nickel- and DNA-bound DtxR(C102D), nickel- and DNA-bound DtxR(C102D) [1DDN (1)], and metal-free DtxR(H79A) [1P92 (23)]} using DALI (distant matrix alignment) (30), show rms deviations on the order of 0.5 Å, indicating similar overall conformations for all of them (1, 5, 23, 26–29).

The electron density in the N-terminal region of Ni-DtxR(H79A,C102D) at a contour level of 6.0σ indicates that there is only one Ni^{2+} ion present at binding site 2 (primary). This binding site is formed by His-106 Nε, Glu-105 Oε, Met-10 S, Asp-102 O (backbone carbonyl), Asp-102 Oδ, and a water molecule that completes the octahedral geometry. The conformation of binding site 2 (primary) of Ni-DtxR(H79A,C102D) was compared with those of metal-bound Ni-DtxR(C102D) and the metal- and DNA-bound Ni-DtxR(C102D)-DNA and Co-DtxR-DNA (1, 5, 29). These latter three structures are examples of the active form of DtxR. Binding site 2 (primary) of Ni-DtxR(H79A,C102D) shows the same conformation found in these structures, suggesting that it is not affected by either the C102D or the H79A mutation, or the presence or absence of DNA (1, 5, 29). The observed distances between the metal ion and the contributing ligands for Ni-DtxR(H79A,C102D), Ni-DtxR(C102D), and Ni-DtxR(C102D)-DNA are presented in Table 2.

The effect of a single mutation to binding site 1 (ancillary) was examined by looking at the structure of DtxR(H79A) (23). Comparison of the structure of Ni-DtxR(H79A,C102D) with that of DtxR(H79A) shows that the positions of the ligands that constitute binding site 2 (primary) of Ni-DtxR(H79A,C102D) are significantly different from those found in the structure of the single binding site 1 (ancillary) mutant DtxR(H79A) (23). The only exception is the carbonyl oxygen of residue 102 whose position is constant in both structures. The largest discrepancy of any of the ligands is found for the side chain of Met-10, where the deviation of the position of the sulfur atom in the single mutant with respect to that of the double mutant is ≈3.4 Å. The other participating binding site 2 (primary) ligands show changes in positions of the coordinating atoms on the order of 1–2 Å. DtxR(H79A) also shows some extraneous electron density around the side chain of Cys-102. This observation was the first clear indication that Cys-102 in DtxR(H79A) had become derivatized during crystallization. This phenomenon has been observed previously in structures of WT DtxR determined in our laboratory and had been overcome by replacement of Cys-102 with Asp (5).

To determine whether the extraneous electron density observed is the result of a group covalently attached to Cys-102, and, if so, what the nature of the species is, we recorded the electrospray ionization–MS spectrum of a sample of DtxR(H79A) from one of the crystals. The mass spectrum of the derivatized DtxR(H79A) mutant gave a molecular mass of 25,326.5 Da, which is 78 Da heavier than expected according to the sequence. The observed difference in molecular mass combined with the shape of the electron density adjacent to Cys-102 in the structure of DtxR(H79A), suggests that 2-mercaptoethanol (78.1 Da) a reducing agent added to the samples, is responsible for the observed chemical modification. Including 2-mercaptoethanol in the crystallographic model of DtxR(H79A) accounts for all of the extraneous electron density adjacent to Cys-102 and leads to a dramatic improvement of refinement statistics (see Fig. 1). It has been observed that during sample manipulation, Cys-102 of WT DtxR is able to react with 2-mercaptoethanol to form a derivative that presumably blocks the binding site and prevents metal ion from binding (31).

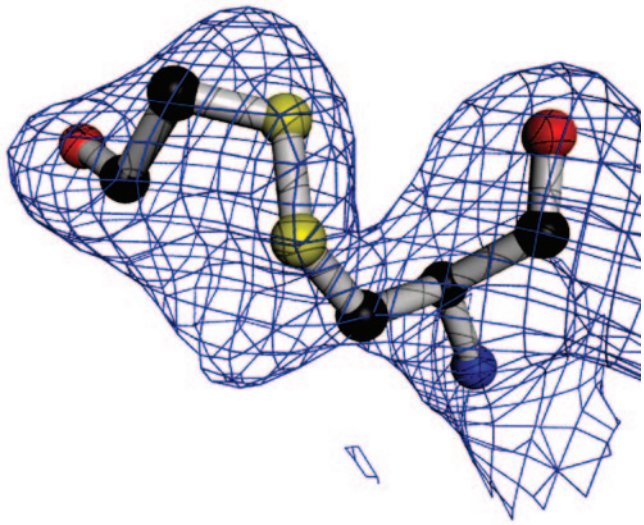

Fig. 1. Electron density of an omit map covering 2-mercaptoethanol coordinated to Cys-102 in the structure of DtxR(H79A). All figures were generated by using MOLSCRIPT, POVSCRIPT+ (38, 39).

Comparison of the structure of the metal ion-bound Ni-DtxR(H79A,C102D) with the metal ion-bound mutant Ni-DtxR(C102D), and the metal- and DNA-bound complex Ni-DtxR(C102D)-DNA shows that the main differences found in the N-terminal region of these structures are located around binding site 1 (ancillary) (1, 5). Binding site 1 (ancillary) of Ni-DtxR(H79A,C102D) can be superimposed on that of the metal-free DtxR(H79A). These structures show an empty site whose open conformation is similar to that observed in metal-free WT DtxR (23) (see Fig. 2), and differences observed can be attributed to the replacement of His-79 by Ala. Although no metal ion was coordinated to binding site 1 (ancillary) in either Ni-DtxR(H79A,C102D) or metal-free DtxR(H79A), replacement of Cys-102 by Asp does not seem to affect the conformation of binding site 1 (ancillary). Therefore, we conclude that the conformational changes observed between Ni-DtxR(H79A,C102D) and metal-free DtxR(H79A) are the result of metal ion binding to binding site 2 (primary) and are not directly produced by the mutations.

Overall, the N-terminal domain of Ni-DtxR(H79A,C102D) has a similar conformation to that found in the structures of Ni-DtxR(C102D) and Ni-DtxR(C102D)-DNA. The first six residues of the N-terminal α-helix of Ni-DtxR(H79A,C102D) are unraveled, a characteristic that is shared by other metal ion-bound and metal ion-bound-DNA-bound structures of DtxR carrying the C102D mutation (1, 5). A key feature shown by the structure of Ni-DtxR(H79A,C102D) is the presence of a water molecule completing the octahedral geometry of binding site 2 (primary). This

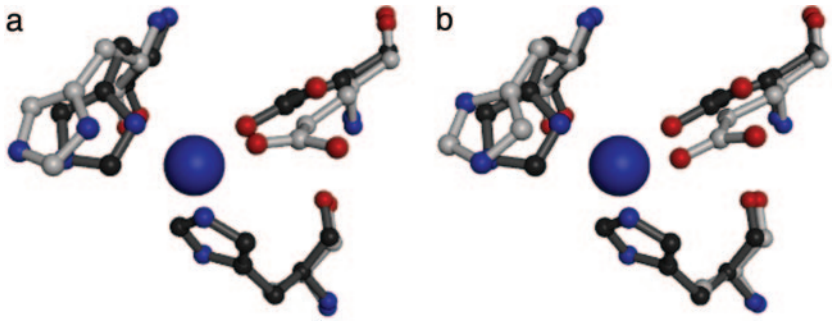

Fig. 2. Comparison of binding site 1 (ancillary) of Ni-DtxR(H79A,C102D) and DtxR(H79A) with DtxR(C102D) (5). (*a*) Structure of DtxR(H79A,C102D) is shown in white, and WT is shown in gray. (*b*) Structure of DtxR(H79A) is shown in white, and WT is shown in gray. Binding site 1 (ancillary) of both mutants show identical open geometry because of the absence of metal ion.

interaction also is observed in the structure of Ni-DtxR(C102D), Ni-DtxR(C102D)-DNA, and that of the structural and functional homologue from *Mycobacterium tuberculosis*, IdeR (1, 32, 33). This interaction connects the carbonyl oxygen of Leu-4 and the metal ion bound to binding site 2 (primary), leaving Val-5 in an unfavorable conformation (1, 32, 33). Because Ni-DtxR(H79A,C102D) has metal ion bound only to binding site 2 (primary), it would seem that the conformational changes observed in the structure, namely the unfolding of the first turn of the N-terminal helix and the unfavorable conformation found for Val-5, are linked to metal ion binding in binding site 2 (primary). The resulting conformational change seems to be necessary for the interaction between the repressor and its operator DNA, because an intact N-terminal α-helix would sterically hinder DNA binding (1, 32).

In summary, because the structure of Ni-DtxR(H79A,C102D) has metal bound only to binding site 2 (primary) and has no other structural changes than those resulting from the H79A mutation, we have concluded that metal ion binding in binding site 2 (primary) is solely responsible for the conformational changes observed. In addition, under our conditions, the structure of the metal-free DtxR(H79A) is superimposable with the metal-free form of WT DtxR. Lacking metal ion in both binding sites, the N-terminal region of DtxR(H79A) does not show any of the conformational changes associated with activation by metal ion.

Binding Affinities. The functional effects of mutations in both DtxR metal-ion binding sites were studied by using a reporter construct in which the diphtheria toxin promoter–operator sequence was fused to the β-galactosidase (β-gal) gene. Early β-gal expression assays of the DH5α:λRS45*tox*PO/*lacZ* fusion construct transformed with plasmids containing WT DtxR and the mutants of binding site 1 (ancillary) [DtxR(H79A), DtxR(E83A), and DtxR(H98A)] and those of binding site 2 (primary) [DtxR(M10A), DtxR(E105A), and DtxR(H106A)], show that although single Ala substitutions of ligands to binding site 2 (primary) have a large effect on the activity of the repressor, single Ala substitution to ligands of binding site 1 (ancillary) did not have a marked effect (5). Gel shift assays of DtxR and single Ala site 1 (ancillary) substitution mutants DtxR(E89A), DtxR(H79A), and DtxR(H98A) incubated with ^{32}P-labeled tox promoter-operator DNA show that, although all of the Ala substitution mutants bind the tox operator, their gel shift is less pronounced than that of WT DtxR (5). Later, *in vivo* experiments using *E. coli* DH5α and SG22098 constructs containing *tox-lac*Z gene fusion confirmed the results obtained by Ding *et al.* (5) for the single Ala substitutions, and showed that double Ala substitutions of ligands of binding site 1 (ancillary), such as DtxR(H79A,E83A) and DtxR(H79A,H98A), have a comparable effect on repressor activity as single Ala substitutions of ligands of binding site 2 (primary), i.e., DNA binding was abolished (6).

This evidence shows that DtxR(H79A) is active *in vivo* and binds DNA *in vitro*. However, the crystal structure of DtxR(H79A) shows no metal ion coordination to either binding site, even at concentrations of metal ion of 5 mM ($NiCl_2$). At this concentration, the active site mutant DtxR(C102D) has both binding sites saturated (5, 34). Because of the observed derivatization of Cys-102 in DtxR(H79A), we did not expect binding site 2 (primary) to be occupied in the crystal structure. Because *in vivo* a minimum of two Ala substitutions are required to abolish activity, the lack of coordination of metal ion in binding site 1 (ancillary) came initially as a surprise. All crystal structures of DtxR solved in our laboratory show only three protein ligands contributing to binding site 1 (ancillary), for which it would be reasonable that the H79A mutation would lead to an empty binding site. A different situation is seen for DtxR(H79A,C102D) whose crystal structure shows metal ion coordination in binding site 2 (primary) only, which would be enough to activate the repressor if metal ion coordination at this site were the only requirement for activation. However, DtxR(H79A,C102D) is not active *in vivo* under the same conditions used to assay DtxR(H79A) (J.A.D., J. F. Love, J.T.-N., J. R. Murphy, and D.R., unpublished data). Because of this apparent inconsistency between structural and biochemical data, it became essential to study metal ion binding to the repressor in solution in a more rigorous fashion to establish the correct number of binding sites required for activation and the order in which they become occupied.

We have obtained the occupancy and relative binding affinities for each of the binding sites using isothermal titration calorimetry. This technique provides an excellent way to determine binding energetics in complex systems and can be used in conjunction with statistical models to assess the number of binding sites that are occupied and the potential cooperativity between them.

Fig. 3 shows the typical shape of the titration curve and the fit to a two binding site model for WT DtxR under the conditions of our experiments. Titration of the other mutants studied show similar binding isotherms (results not shown). The relative binding affinities determined for WT DtxR and the mutants DtxR(H79A), DtxR(C102D), and DtxR(H79A,C102D) for Ni^{2+} are shown in Table 3. The titration of DtxR and all of the mutants used in this work is best described by a model consisting of two occupied binding sites, one of high affinity and one of low affinity. Under our experimental conditions, WT DtxR has a high-affinity binding site (1.7×10^{-7}) and a low-affinity binding site (6.4×10^{-4}). Replacement of His by Ala in DtxR(H79A) lowers the binding affinity of the high-affinity binding site by one order of magnitude but does not affect the affinity of the low-affinity binding site beyond the experimental error. Similarly, replacement of Cys-102 by Asp in DtxR(C102D) shows a decrease of one order of magnitude in the binding affinity of the low-affinity binding site. The binding affinities of DtxR(H79A,C102D) show a decrease of approximately one order of magnitude for each of the binding sites.

These results are consistent with binding site 1 (ancillary) being the high-affinity binding site and the first one to be occupied under the conditions of these experiments. It is worth noting that *in vitro*, in the absence of any other effect, both binding sites can be saturated as long as a sufficiently high concentration of metal ion is supplied, whereas *in vivo* the maximal concentration of metal ion

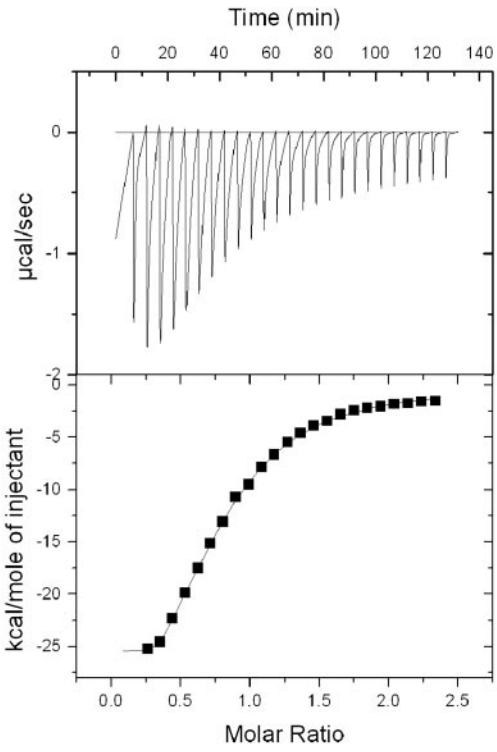

Fig. 3. Calorimetric titration of WT DtxR (64 μM) with 1 mM $NiCl_2$. *Upper* shows the actual heat associated with each injection. *Lower* shows the data fitted to a two-binding site model. Other mutants of DtxR studied produced similar curves and fits.

available is fixed. In the case of typical *E. coli* cells, the total concentration of ferrous ion, which is the physiologically active metal ion for DtxR, has been estimated to be 0.1 mM using data of Finney and O'Halloran (35) for the total number of ferrous ions and the cell volume estimated in Cayley *et al.* (36). However, the actual free iron concentration is unknown, as is the redox state and the corresponding values in *Corynebacterium diphtheria*. If the binding affinity of binding site 2 (primary) of DtxR(H79A,C102D) for ferrous ion is similar to what we have measured for nickel, the total available concentration of ferrous ion inside a typical *E. coli* cell might not be high enough to saturate both binding sites and, in view of the observed decrease in binding affinity, could explain why DtxR(H79A,C102D) is not active *in vivo*. Similarly, as our results indicate, the single H79A mutation does not prevent metal ion binding to binding site 1 (ancillary) in solution, although it does lower binding affinity, and does not affect the binding affinity of binding site 2 (primary) at all. Such differential binding affinities could explain why DtxR(H79A) remains active *in vivo*. In fact, *in vivo*, a minimum of two Ala substitutions in binding site 1 (ancillary) are required to abolish activity of the repressor (6).

The structures of the metal-free DtxR(H79A), Ni-DtxR(C102D), and Ni-DtxR(H79A,C102D) show that these mutations do not disrupt the binding sites enough to prevent metal ion

Table 3. Binding affinities of DtxR for Nickel II at 298K determined by ITC

Protein	High-affinity binding site	Low-affinity binding site
DtxR WT	1.7×10^{-7}	6.4×10^{-4}
DtxR(H79A)	1.1×10^{-6}	5.7×10^{-4}
DtxR(C102D)	5.5×10^{-6}	6.6×10^{-3}
DtxR(H79A,C102D)	1.1×10^{-6}	2.5×10^{-3}

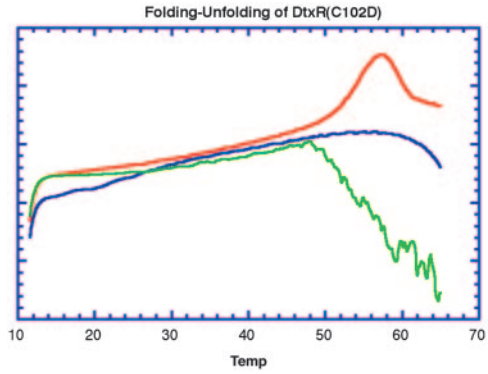

Fig. 4. Thermally induced folding-unfolding transitions of DtxR(C102D) recorded by DSC. The red trace corresponds to apo-DtxR(C102D); a transition is observed at 57.1°C. The green trace corresponds to DtxR(C102D) after incubation with 5 mM $NiCl_2$ and shows aggregation. The blue trace corresponds to apo-DtxR(C102D) at pH 4.5 and shows complete unfolding.

binding (5, 23). The fact that binding site 1 (ancillary) has the highest affinity for metal ion indicates that, under classic thermodynamic control, binding site 1 (ancillary) would be the first one to be occupied. Under the same assumptions, the active repressor must require the presence of a fully occupied binding site 1 (ancillary), and, therefore, the role of binding site 1 in the functionality of DtxR cannot be underestimated. In addition, if binding sites 1 (ancillary) and 2 (primary) of DtxR are correlated, the combined effect of the mutations H79A and C102D on the binding affinities of the double mutant DtxR(H79A,C102D) would be larger than the sum of the individual mutations observed in the corresponding single mutants. However, because our results show the effect of these mutations on the metal-ion binding affinity to be simply additive, the possibility of cooperativity between the two binding sites would seem to be ruled out.

Thermal Stability of DtxR. Because binding site 1 (ancillary) is not directly involved in DNA recognition, a hypothesis for its role is that it increases stability of either the monomer or the dimer of DtxR. DSC provides information about the thermal stability of a system and its oligomerization state. Structural data show that in the crystal, the metal ion-bound and the metal ion- and DNA-bound forms are dimeric and have a similar overall structure, suggesting that DNA is not required for dimerization. Therefore, to study the effect of the metal ion on the oligomerization state of the protein, we measured the folding–unfolding transitions of the system. The experiments presented here were performed using DtxR(C102D), in an attempt to overcome problems of derivatization of Cys-102. However, WT DtxR and all other mutants studied (results not shown) presented similar thermally induced folding–unfolding profiles, albeit with different transition temperatures. At pH 7.5 in the absence of metal ion, the thermal denaturation profile of DtxR(C102D) shows a single transition centered at 57.1°C (see Fig. 4). Because the thermally induced folding–unfolded profile of an oligomeric protein is dependent on the total protein concentration, the oligomerization state of a protein can be tested by carrying out DSC experiments at different protein concentrations (37). In the range of concentrations studied, the transition temperature of metal-free DtxR(C102D) is independent of the protein concentration, indicating that the protein behaves as a monomer. Identical experiments performed at pH 4.5 show no folding–unfolding transition, suggesting that DtxR is unfolded at low pH.

Incubation of the protein sample in 5 mM $NiCl_2$ leads to aggregation before the transition temperature (see Fig. 4). Lower cation or protein concentrations did not reduce the extent of the aggregation. This result suggests that in the presence of metal ion,

a radically different folding–unfolding behavior is taking place. One possibility is that upon addition of metal ion, an interaction between the C- and N-terminal domains, either intramolecularly or intermolecularly, is allowed to occur. Structural data have shown that side chains from two C-terminal residues from a neighboring crystallographic monomer can contribute to the stabilization of binding site 1 (ancillary) of both DtxR and its homologue IdeR (29, 33). This observation has led investigators to believe that this interaction also could be established intramolecularly (7). Although aggregation problems prevented us from reaching our overall goal of determining the transition temperature of the system in the presence of metal ion and whether incubation with the metal ion leads to dimer formation, we observed a dramatic change in behavior that is consistent with such a conformational change.

Because the occupancies of the metal ion in the crystal structures of DtxR(H79A) and DtxR(H79A,C102D) are inconsistent, we studied the thermal stability of the system under identical conditions to those used for crystallization to see whether, under these conditions, the system would experience an increase in stability that could explain the lack of metal ion observed in binding site 1 (ancillary) in the structures of DtxR(H79A) and DtxR(H79A,C102D). Both DtxR(H79A) and DtxR(H79A,C102D) were crystallized at a concentration of 1.4 M $(NH_4)_2SO_4$. Under such nonphysiological conditions, the stability of DtxR may be severely affected, and, as a result, our crystal structures may show conformations that are induced by the crystallization environment rather than intrinsic interactions present in solution. In fact, the N-terminal region of DtxR(H79A) and the Ni-DtxR(H79A,C102D) show similar B-factors, 23 and 32 $Å^2$, respectively, indicating that under the crystallization conditions, it is possible to obtain a well resolved structure of DtxR without having metal ion bound to either binding site. In solution, the folding–unfolding profiles in 1.4 M $(NH_4)_2SO_4$ show an increase in melting temperature of 5.1°C, indicating that it is possible to modulate the stability of the repressor in solution by varying the concentration of salts in solution, even with ions that have not been shown to bind the repressor specifically. NMR experiments of DtxR in solution have demonstrated that metal ion binding leads to a more ordered protein (12). Given that a metal ion binds to binding site 1 (ancillary) first, and that a structure of the repressor can be obtained in the absence of metal ion. (26), it would seem that metal ion binding to site 1 (ancillary) can be replaced by an increased salt concentration, leading to stabilization of the protein structure. We therefore suggest that the role of binding site 1 is to stabilize the structure.

A Working Model. The combined use of calorimetric and crystallographic techniques presented in this work has increased our understanding of the role of each metal ion-binding site at the molecular level and has provided a clearer picture of the order in which different events take place during metal ion activation of DtxR. The activation mechanism can be summarized as follows: at low concentrations of metal ion, DtxR exists essentially as a monomer. As the concentration of metal ion increases, DtxR binds metal ion in a sequence determined by the binding affinities, with binding site 1 (ancillary) becoming occupied first stabilizing the monomer. There are no significant conformational changes in the N-terminal region of the repressor associated with metal ion binding to site 1 (ancillary) under the conditions of our experiment. Once binding site 1 (ancillary) is occupied, metal ion is then able to bind to binding site 2 (primary) when the metal ion concentration is sufficiently high. At this stage, small conformational changes take place in the N-terminal region. The first six residues of N-terminal helix unravel allowing the water-mediated interaction between the carbonyl oxygen of Leu-4 and binding site 2 (primary) metal ion to occur. Once the repressor is activated, dimerization can occur and the repressor is able to interact with its operator DNA.

We thank Dr. John R. Murphy for providing proteins and plasmids used in this work and Dr. Michael Marletta for helpful discussions. Mass spectral data were provided by the Boston University School of Medicine Mass Spectrometry Resource, which is supported by National Institutes of Health (NIH)/National Center for Research Resources Grant P41-RR10888 and NIH Grant S10-RR10493 (to C. E. Costello, Boston University, Boston). Synchrotron data were collected at beamline X12C of the National Synchrotron Light Source at Brookhaven National Laboratory during the RapiData 2001 course. This work was supported NIH Grant AI21628 (to John R. Murphy and D.R.). We also thank the Biophysical Instrumentation Facility for the Study of Complex Macromolecular Systems at MIT (National Science Foundation Grant NSF-0070319 and NIH Grant GM68762).

1. White, A., Ding, X. C., vanderSpek, J. C., Murphy, J. R. & Ringe, D. (1998) *Nature* **394,** 502–506.
2. Qiu, X. Y., Verlinde, C., Zhang, S. P., Schmitt, M. P., Holmes, R. K. & Hol, W. G. J. (1995) *Structure (London)* **3,** 87–100.
3. Rangachari, V., Marin, V., Bienkiewicz, E. A., Semavina, M., Guerrero, L., Love, J. F., Murphy, J. R. & Logan, M. T. (2005) *Biochemistry* **44,** 5672–5682.
4. Posey, J. E., Hardham, J. M., Norris, S. J. & Gherardini, F. C. (1999) *Proc. Natl. Acad. Sci. USA* **96,** 10887–10892.
5. Ding, X., Zeng, H., Schiering, N., Ringe, D. & Murphy, J. R. (1996) *Nat. Struct. Biol.* **3,** 382–387.
6. Goranson-Siekierke, J., Pohl, E., Hol, W. G. J. & Holmes, R. K. (1999) *Infect. Immun.* **67,** 1806–1811.
7. Love, J. F., vanderSpek, J. C. & Murphy, J. R. (2003) *J. Bacteriol.* **185,** 2251–2258.
8. Spiering, M. M., Ringe, D., Murphy, J. R. & Marletta, M. A. (2003) *Proc. Natl. Acad. Sci. USA* **100,** 3808–3813.
9. Tao, X. & Murphy, J. R. (1992) *J. Biol. Chem.* **267,** 21761–21764.
10. Wang, Z. O., Schmitt, M. P. & Holmes, R. K. (1994) *Infect. Immun.* **62,** 1600–1608.
11. Tao, X., Zeng, H. Y. & Murphy, J. R. (1995) *Proc. Natl. Acad. Sci. USA* **92,** 6803–6807.
12. Twigg, P. D., Parthasarathy, G., Guerrero, L., Logan, T. M. & Caspar, D. L. D. (2001) *Proc. Natl. Acad. Sci. USA* **98,** 11259–11264.
13. Otwinowski, Z. & Minor, W. (1997) *Macromol. Crystallogr. A* **276,** 307–326.
14. Pflugrath, J. W. (1999) *Acta Crystallogr. D* **55,** 1718–1725.
15. Kissinger, C. R., Gehlhaar, D. K. & Fogel, D. B. (1999) *Acta Crystallogr. D* **55,** 484–491.
16. Brunger, A. T., Adams, P. D., Clore, G. M., DeLano, W. L., Gros, P., Grosse-Kunstleve, R. W., Jiang, J. S., Kuszewski, J., Nilges, M., Pannu, N. S., *et al.* (1998) *Acta Crystallogr. D* **54,** 905–921.
17. Jones, T. A., Zou, J. Y., Cowan, S. W. & Kjeldgaard, M. (1991) *Acta Crystallogr. A* **47,** 110–119.
18. Brunger, A. T. (1992) *Nature* **355,** 472–475.
19. Laskowski, R. A., Macarthur, M. W., Moss, D. S. & Thornton, J. M. (1993) *J. Appl. Crystallogr.* **26,** 283–291.
20. Morris, A. L., Macarthur, M. W., Hutchinson, E. G. & Thornton, J. M. (1992) *Proteins Struct. Funct. Genet.* **12,** 345–364.
21. Hodel, A., Kim, S. H. & Brunger, A. T. (1992) *Acta Crystallogr. A* **48,** 851–858.
22. Chen, C. S. Y., White, A., Love, J., Murphy, J. R. & Ringe, D. (2000) *Biochemistry* **39,** 10397–10407.
23. D'Aquino, J. A. & Ringe, D. (2003) *J. Bacteriol.* **185,** 4081–4086.
24. Ramachandran, G. N., Ramakrishnan, C. & Sasisekharan, V. (1963) *J. Mol. Biol.* **7,** 95–99.
25. McCaldon, P. & Argos, P. (1988) *Proteins Struct. Funct. Genet.* **4,** 99–122.
26. Schiering, N., Tao, X., Zeng, H. Y., Murphy, J. R., Petsko, G. A. & Ringe, D. (1995) *Proc. Natl. Acad. Sci. USA* **92,** 9843–9850.
27. Pohl, E., Holmes, R. K. & Hol, W. G. J. (1998) *J. Biol. Chem.* **273,** 22420–22427.
28. Qiu, X. Y., Pohl, E., Holmes, R. K. & Hol, W. G. J. (1996) *Biochemistry* **35,** 12292–12302.
29. Pohl, E., Holmes, R. K. & Hol, W. G. J. (1999) *J. Mol. Biol.* **292,** 653–667.
30. Holm, L. & Sander, C. (1993) *J. Mol. Biol.* **233,** 123–138.
31. Tao, X., Schiering, N., Zeng, H. Y., Ringe, D. & Murphy, J. R. (1994) *Mol. Microbiol.* **14,** 191–197.
32. Pohl, E., Goranson-Siekierke, J., Choi, M. K., Roosild, T., Holmes, R. K. & Hol, W. G. J. (2001) *Acta Crystallogr. D* **57,** 619–627.
33. Feese, M. D., Ingason, B. P., Goranson-Siekierke, J., Holmes, R. K. & Hol, W. G. J. (2001) *J. Biol. Chem.* **276,** 5959–5966.
34. Tao, X. & Murphy, J. R. (1993) *Proc. Natl. Acad. Sci. USA* **90,** 8524–8528.
35. Finney, L. A. & O'Halloran, T. V. (2003) *Science* **300,** 931–936.
36. Cayley, D. S., Guttman, H. J. & Record, M. T. (2000) *Biophys. J.* **78,** 1748–1764.
37. Freire, E. (1989) *Comm. Mol. Cell Biophys.* **6,** 123–140.
38. Kraulis, P. J. (1991) *J. Appl. Crystallogr.* **24,** 946–950.
39. Fenn, T. D., Ringe, D. & Petsko, G. A. (2003) *J. Appl. Crystallogr.* **36,** 944–947.